

Phase Separation of Ternary Mixtures: Symmetric Polymer Blends

C. Huang,^{*†} M. Olvera de la Cruz,^{†‡} and B. W. Swift[†]

Department of Materials Science and Engineering, Northwestern University, Evanston, Illinois 60208, and CEA Service de Chimie Moléculaire, CE-SACLAY, 91191 Gif sur Yvette Cedex, France

Received April 11, 1995; Revised Manuscript Received July 31, 1995[§]

ABSTRACT: The dynamics of phase separation of ternary mixtures into two and three phases are analyzed numerically by solving the nonlinear spinodal decomposition equations in two dimensions. We find interesting interface effects during the decomposition process. Between any two $\alpha + \beta$ phases rich in components I and J respectively, the third component K segregates in the interface between α and β . We study the interface segregation effects in symmetric ternary polymer blends (i.e., with equal Flory interaction parameters between each pair of monomers and equal degrees of polymerization). This segregation phenomenon influences strongly the growth of a third phase with lowest equilibrium volume fraction. In the absence of hydrodynamics, the kinetics of the minority phase is determined by the topology of the segregation pattern initiated by the decomposition of the most unstable phases. Coarsening of the minority phase occurs at the junction of four or more majority phase domain boundaries. We examine the dynamical scaling and the growth laws for the late stages of separation into two and three phases. The growth law $R(\tau) \sim \tau^{1/3}$ is always obeyed even when the structures are not self-similar. The self-similar regime is achieved very slowly in ternary systems.

I. Introduction

For many years blending polymers with a high degree of polymerization has been of commercial interest since it may lead to new materials with more favorable performance than the pure components. Most polymer mixtures are immiscible leading to the formation of multiple phases. Therefore it is important to study the phase behavior for polymer blends. While phase separation has been extensively studied in binary systems,¹ only a few studies exist in multicomponent systems.^{2,3} In this paper we describe phase separation in ternary polymer blends.

We study immiscible blends of long, highly flexible molecules, which obey Gaussian statistics in the molten state.⁴ We construct the free energy of the blends using the simplest mean field model, the Flory–Huggins–de Gennes free energy, which de Gennes pointed out describes properly immiscible high degree of polymerization polymer blends.^{5,6} The immiscibility between components I and J in polymer blends is described by the Flory interaction parameter, χ_{IJ} , which is generally positive and favors segregation. For example, above a critical value of $\chi_{AB} = 2/N$ a symmetric A–B binary system of degree of polymerization N separates into two phases.^{7,8} When a system is unstable against infinitesimal fluctuations in composition, the separation process is termed spinodal decomposition.

The phase behavior of ternary polymer blends, however, is more complicated. These systems can decompose into two or three phases. In this paper we study the kinetics of phase separation when the mixture decomposes into two and three phases. We find that between any two phases rich in components I and J, the third component K segregates in the interface, even when the equilibrium composition of the third component K is equal in both phases. This interface segregation phenomenon influences the decomposition patterns into two and three phases in ternary systems.

We also explore the dynamical scaling and the growth behaviors in ternary systems, which have been widely accepted in binary systems. In binary systems the decomposition pattern into two phases is generally bicontinuous. The resulting structure is self-similar.¹ The structure function $S(k,\tau)$, accessible by the scattering radiation experiments, scales as $(R(\tau))^d G(kR(\tau))$ where $R(\tau)$ is associated with the domain size, d is the space dimensionality, and G is a function independent of time. The bicontinuous structure coarsens asymptotically in time according to the growth law $R \sim \tau^{1/3}$. Recently this *universality* in the scaling and the growth behaviors was observed in ternary mixtures with symmetric compositions, i.e., $\bar{\varphi}_I = 1/3$, $I = A, B, C$, decomposing into three phases.³ In these systems, however, the segregation of the third component along the interface was not observed. Here we find that even when there is segregation along the interface, the growth law is always obtained, the scaling regime, however, is reached in the very late stages of the decomposition process.

For simplicity, we study symmetric A–B–C ternary polymer blends, i.e., $\chi_{AB} = \chi_{BC} = \chi_{AC} = \chi$ and $N_A = N_B = N_C = N$. We numerically solve the nonlinear diffusion equations during spinodal decomposition, extending the method used to study binary systems⁹ to ternary blends. In section II we outline the mean field thermodynamics of ternary polymer blends, from which the phase diagrams for symmetric ternary polymer blends are constructed. In section III the dynamic model and the techniques for numerically solving the diffusion equations are described. The decomposition patterns are given and discussed in section IV.a, and the dynamical scaling and the growth laws are investigated in section IV.b. The conclusions of our studies are given in section V.

II. Thermodynamic Analysis

The Flory–Huggins–de Gennes mean field free energy per site of an A–B–C ternary polymer blend is given by

$$\Delta f = \Delta f_0 + \sum_{I=A,B,C} \bar{\kappa}_{II} (\nabla \varphi_I)^2 \quad (II.1a)$$

^{*} Northwestern University.

[†] CEA Service de Chimie Moléculaire.

[‡] Abstract published in *Advance ACS Abstracts*, November 1, 1995.

where Δf° is the regular solution model free energy per site. Δf° is a functional of the local compositions of component I, $\varphi_I(r)$, I = A, B, and C,

$$\frac{\Delta f^\circ}{k_B T} = \frac{\varphi_A \ln \varphi_A}{N_A} + \frac{\varphi_B \ln \varphi_B}{N_B} + \frac{\varphi_C \ln \varphi_C}{N_C} + \chi_{AB}\varphi_A\varphi_B + \chi_{BC}\varphi_B\varphi_C + \chi_{AC}\varphi_A\varphi_C \quad (\text{II.1b})$$

where N_I is the degree of polymerization of component I, I = A, B, C. The blend is assumed to be incompressible: $\varphi_A(r) + \varphi_B(r) + \varphi_C(r) = 1$. The gradient energy term coefficients $\bar{\kappa}_{II}$ in blends are computed using the Random Phase Approximation:¹⁰

$$\bar{\kappa}_{II} = k_B T(a^2/36\bar{\varphi}_I) \quad (\text{II.2})$$

where a is the monomer size and $\bar{\varphi}_I$ is the mean composition of I in the whole system.¹¹ (For simplicity $\bar{\kappa}_{II}$ is assumed to be independent of the local composition $\varphi_I(r)$, this approximation, however, does not affect the results obtained here.¹²)

The equilibrium state of the system is determined by equating the chemical potential of each component I, $\mu_{\circ,I}^m$, in the possible coexisting phases m, m = α, β, γ , including the mass conservation laws, i.e.,

$$\mu_{\circ,I}^\alpha = \mu_{\circ,I}^\beta = \mu_{\circ,I}^\gamma \quad I = A, B, C \quad (\text{II.3a})$$

$$\bar{\varphi}_I = \nu^\alpha \bar{\varphi}_I^\alpha + \nu^\beta \bar{\varphi}_I^\beta + \nu^\gamma \bar{\varphi}_I^\gamma \quad I = A, B, C \quad (\text{II.3b})$$

where ν^m is the volume fraction of phase m and $\bar{\varphi}_I^m$ is the mean composition of I in the m phase. The chemical potential is defined as the change of the total free energy ΔF° with respect to the number of component I, n_I , without the gradient energy terms,

$$\mu_{\circ,I} = \frac{\partial \Delta F^\circ}{\partial n_I} \quad (\text{II.4a})$$

It has the form of (see Appendix A)

$$\begin{aligned} \mu_{\circ,I} = k_B T(\ln \bar{\varphi}_I + 1 - \bar{\varphi}_I - \sum_{J \neq I} \bar{\varphi}_I(N_I/N_J) + \\ \sum_{J \neq I} \chi_{IJ} N_I \bar{\varphi}_J (1 - \bar{\varphi}_I) - \chi_{KL} N_I \bar{\varphi}_K \bar{\varphi}_L) \end{aligned} \quad (\text{II.4b})$$

$$(I \neq K \neq L, I, J, K' = A, B, C)$$

For ternary systems the spinodal curves (the limits of instability of the homogeneous phase) are determined by¹³

$$\begin{vmatrix} f_{AA} & f_{AB} \\ f_{BA} & f_{BB} \end{vmatrix} = 0 \quad (\text{II.5})$$

with

$$f_{IJ} = \left(\frac{\partial}{\partial \varphi_I} - \frac{\partial}{\partial \varphi_C} \right) \left(\frac{\partial}{\partial \varphi_J} - \frac{\partial}{\partial \varphi_C} \right) \Delta f^\circ, \quad I, J = A, B \quad (\text{II.6a})$$

By eqs II.1b and II.6a

$$f_{II} = \frac{1}{\bar{\varphi}_I N_I} + \frac{1}{\bar{\varphi}_C N_C} - 2\chi_{IC} \quad I = A, B \quad (\text{II.6b})$$

$$f_{AB} = f_{BA} = \frac{1}{\bar{\varphi}_C N_C} + \chi_{AB} - \chi_{AC} - \chi_{BC} \quad (\text{II.6c})$$

The phase diagrams and the spinodal curves for symmetric ternary polymer blends, $\chi_{AB} = \chi_{BC} = \chi_{AC} = \chi$ and $N_A = N_B = N_C = N$, calculated using eqs II.3 and II.5 are shown in ABC composition triangles for different χN values. The I-th corner in the triangle represents a system of 100% of component I. For $\chi N < 2$, the ternary system is homogeneous at any composition ($\bar{\varphi}_A, \bar{\varphi}_B, \bar{\varphi}_C$) in the triangle ABC. A typical ternary phase diagram for $2 \leq \chi N < 2.57$ is given in Figure 1a where $\chi N = 2.4$. In the diagram the A-rich, B-rich, and C-rich phases are labeled as α, β , and γ , respectively, and the one-phase region around the center of the composition triangle is labeled as δ . As χN increases from 2.0 to 2.57 we find three lines of critical points given by $[1/\chi N, 1/\chi N, 1-2/\chi N]$, $[1-2/\chi N, 1/\chi N, 1/\chi N]$, and $[1/\chi N, 1-2/\chi N, 1/\chi N]$. We show the three critical points at $\chi N = 2.4$ in Figure 1a; they are determined by the intersection of the spinodal lines with the coexistence curves in each $\alpha + \beta$, $\beta + \gamma$, and $\alpha + \gamma$ region. The tie lines, which give the equilibrium compositions in the two-phase regions, are parallel to the I-J axis. For example, for any composition along the DE line the equilibrium compositions are given by $D = (\bar{\varphi}_A^\alpha, \bar{\varphi}_B^\alpha, \bar{\varphi}_C)$, and $E = (\bar{\varphi}_A^\beta, \bar{\varphi}_B^\beta, \bar{\varphi}_C)$.

When $\chi N > 2.57$ three-phase regions appear in the phase diagrams. There are six three-phase regions shown inside small triangles in Figure 1b where $\chi N = 2.65$. As expected by phase rules, each three-phase region is separated from the single phase regions by the two-phase regions on the right and left of each small triangle. These six new two-phase regions each have a critical point (as χN increases, they generate six lines of critical points emerging from the critical points at $\chi N = 2.57$). For example, for any initial composition inside the triangle HKL, with equilibrium compositions given by $H = (\bar{\varphi}_A^\alpha, \bar{\varphi}_B^\alpha, \bar{\varphi}_C^\alpha)$, $K = (\bar{\varphi}_A^\beta, \bar{\varphi}_B^\beta, \bar{\varphi}_C^\beta)$, and $L = (\bar{\varphi}_A^\delta, \bar{\varphi}_B^\delta, \bar{\varphi}_C^\delta)$, the left and right of the triangle HKL are $\alpha + \delta$ and $\beta + \delta$, respectively. When $\chi N = 8/3$, the critical lines of $\alpha + \delta$, $\beta + \delta$, and $\gamma + \delta$ join at $(0.5, 0.25, 0.25)$, $(0.25, 0.5, 0.25)$, and $(0.25, 0.25, 0.5)$, respectively as shown in Figure 1c. For $\chi N > 8/3$ these two-phase regions overlap and all the critical points disappear as shown in Figure 1d for $\chi N = 2.7$. When χN is 2.7456, the three-phase regions shown in Figure 1d touch at the center of the ABC triangle (see Figure 1e). For $\chi N > 2.7456$ they overlap leading to a single interior α, β , and γ three-phase triangle with equilibrium compositions given by the points X, Y, and Z shown in Figure 1f where $\chi N = 3.0$.

We analyze systems which are symmetric in A and B, i.e., systems along a line perpendicular to the A-B axis such as points 1, 2, and 3 in Figure 1d, and points 4 and 5 in Figure 1f. In ternary systems with $\bar{\varphi}_A = \bar{\varphi}_B$, it is convenient to expand the free energy Δf° in two order parameters $\psi_1(r)$ and $\psi_2(r)$ given by

$$\psi_1(r) = \frac{1-f}{\bar{\varphi}} \delta \varphi_A(r) - \frac{f}{\bar{\varphi}} \delta \varphi_B(r) \quad (\text{II.7a})$$

$$\psi_2(r) = \delta \varphi_A(r) + \delta \varphi_B(r) \quad (\text{II.7b})$$

with $\bar{\varphi} = \bar{\varphi}_A + \bar{\varphi}_B$, $f = \bar{\varphi}_A/\bar{\varphi}$, and $\delta \varphi_I(r) = \varphi_I(r) - \bar{\varphi}_I$. $\psi_2(r) = 0$ if C is homogeneous. If we expand Δf° in terms of ψ_1 and ψ_2

$$\Delta f^\circ \propto \Gamma_{11}\psi_1^2 + \Gamma_{22}\psi_2^2 + (\text{higher order terms}) \quad (\text{II.8})$$

where $\Gamma_{11} = [\bar{\varphi}/f(1-f)N] - 2\bar{\varphi}^2\chi$ and $\Gamma_{22} = [1/\bar{\varphi}(1-\bar{\varphi})N] + (2f(1-f) - 2)\chi$. The signs of the coefficients Γ_{11} and Γ_{22} determine the instability of the formation

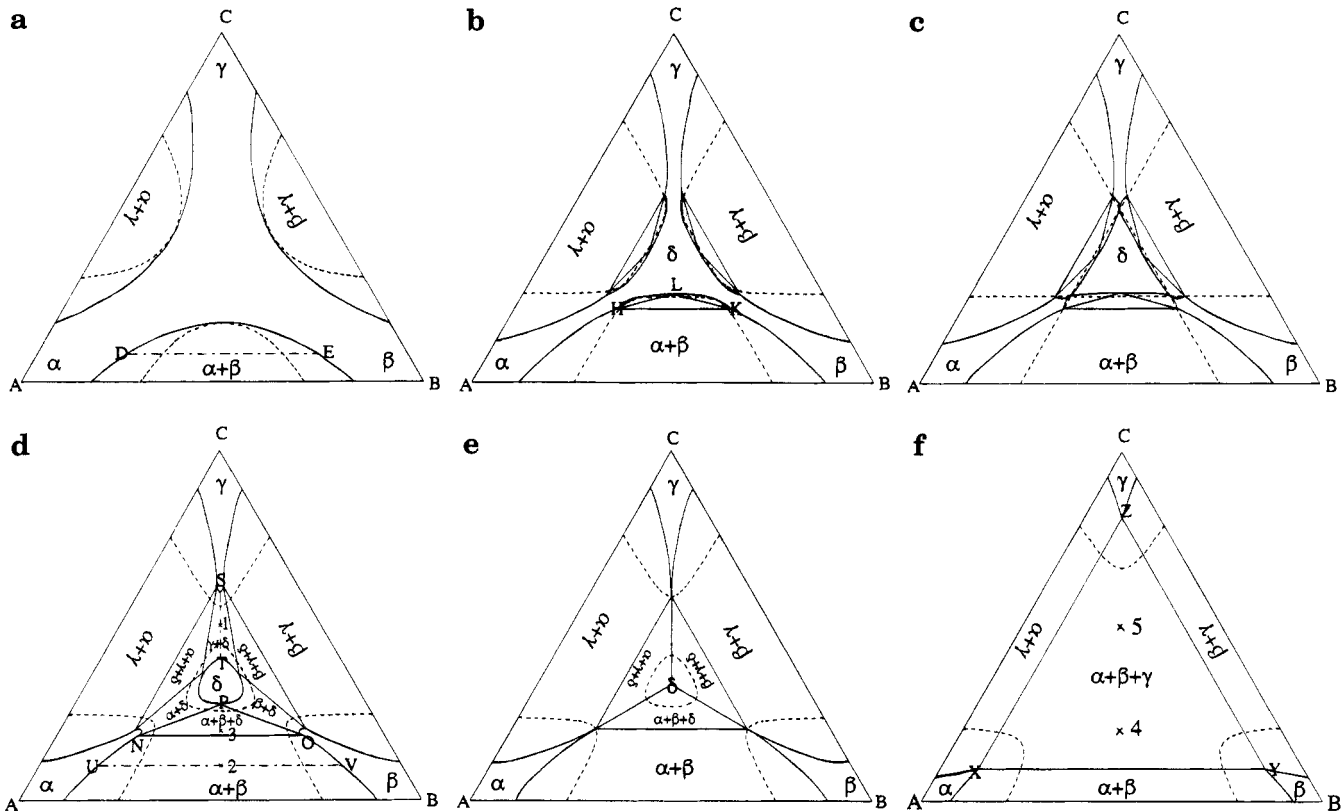


Figure 1. The phase diagrams of symmetric ternary systems for (a) $\chi N = 2.4$, (b) $\chi N = 2.65$, (c) $\chi N = \frac{8}{3}$, (d) $\chi N = 2.7$, (e) $\chi N = 2.7456$, and (f) $\chi N = 3.0$. The symbols (—) and (---) correspond to the spinodal curves and the tie lines, respectively.

of $\alpha + \beta$ and γ , respectively. At point 1 in Figure 1d the system has composition (0.25, 0.25, 0.5) and it is unstable to the formation of γ and δ with $S = (0.202, 0.202, 0.596)$ and $T = (0.298, 0.298, 0.404)$, respectively ($\Gamma_{11} > 0$; $\Gamma_{22} < 0$). At point 2 the composition is (0.45, 0.45, 0.1) and the system is unstable to the formation of α and β with compositions $U = (0.7539, 0.1461, 0.1)$ and $V = (0.1461, 0.7539, 0.1)$, respectively ($\Gamma_{11} < 0$; $\Gamma_{22} > 0$). At point 3 the system has composition (0.4, 0.4, 0.2) and is unstable to the formation of two majority $\alpha + \beta$ phases, and metastable to the formation of one minority δ phase with equilibrium compositions $N = (0.6107, 0.2033, 0.186)$, $O = (0.2033, 0.6107, 0.186)$, and $P = (0.3636, 0.3636, 0.2728)$, respectively ($\Gamma_{11} < 0$; $\Gamma_{22} > 0$). Finally systems at points 4 and 5 in Figure 1f of compositions (0.4, 0.4, 0.2) and (0.25, 0.25, 0.5), respectively, form α , β , and γ phases with compositions $X = (0.811, 0.0945, 0.0945)$, $Y = (0.0945, 0.811, 0.0945)$, and $Z = (0.0945, 0.0945, 0.811)$, respectively. System 4 is unstable to the formation of $\alpha + \beta$ and metastable to the formation of γ ($\Gamma_{11} < 0$; $\Gamma_{22} > 0$); while system 5 is metastable to the formation of $\alpha + \beta$ and unstable to the formation of γ ($\Gamma_{11} > 0$; $\Gamma_{22} < 0$).

III. Dynamic Model and Numerical Methods

The kinetics of spinodal decomposition are described by a continuity equation

$$\partial\varphi_I/\partial t = -\nabla J_I \quad I = A, B, C \quad (\text{III.1})$$

where the flux is proportional to the gradient of the chemical potential of I per site μ_I^s ,

$$J_I = -M_I \nabla \mu_I^s \quad (\text{III.2})$$

where M_I is the Onsager coefficient of I . μ_I^s is determined including the compositional gradient terms in Δf (see Appendix B). We ignore the thermal fluctuations because they are negligible for quenches far away from the critical points and/or spinodal lines,¹⁴ where the driving force for phase separation is much larger than the thermal fluctuations.

In constructing the nonlinear diffusion equation for polymer blends, two theories have been used, one proposed by de Gennes,⁶ and the other by Kramer et al.¹⁵ We adopt the results of Kramer et al. who propose that there is a net vacancy flux during the diffusion process with the constraint of local thermal equilibrium of vacancies, which has been shown¹⁶ to agree better with experiments.¹⁷ The net flux of each component I , J_I , is equal to

$$J_I = J_I + \varphi_I J_V \quad (\text{III.3a})$$

where J_V is the vacancy flux,

$$J_V = -(J_A + J_B + J_C) \quad (\text{III.3b})$$

We eliminate the variable $\varphi_C(r, t)$ using the incompressibility condition and use the Gibbs–Duhem relationship locally, $\sum_{I=A,B,C} \bar{\varphi}_I d\mu_I^s \equiv 0$; eqs III.1 become

$$\begin{aligned} \frac{\partial}{\partial t} [\varphi_I(r, t)] &= M_{II} \nabla^2 (\mu_{I,I}^s - \mu_{I,C}^s - 2\kappa_{II} \nabla^2 \varphi_I - 2\kappa_{IJ} \nabla^2 \varphi_J) + \\ &\quad M_{IJ} \nabla^2 (\mu_{I,J}^s - \mu_{I,C}^s - 2\kappa_{JI} \nabla^2 \varphi_I - 2\kappa_{JJ} \nabla^2 \varphi_J) \\ &\quad I \neq J; I, J = A, B \quad (\text{III.4}) \end{aligned}$$

where $\mu_{I,I}^s = \partial \Delta f / \partial \varphi_I$ is given in eq A.5

$$M_{II} = (1 - \bar{\varphi}_I)^2 M_I + \bar{\varphi}_I^2 \sum_{J=I, J=A, B, C} M_J \quad I = A, B \quad (\text{III.5a})$$

$$M_{AB} = M_{BA} = -(1 - \bar{\varphi}_A)\bar{\varphi}_B M_A - (1 - \bar{\varphi}_B)\bar{\varphi}_A M_B + \bar{\varphi}_A \bar{\varphi}_B M_C \quad (\text{III.5b})$$

$\kappa_{II} = \bar{\kappa}_{II} + \bar{\kappa}_{CC}$, $I = A, B$, and $\kappa_{AB} = \kappa_{BA} = \bar{\kappa}_{CC}$, given in eq II.2. In long polymer blends the mobility is given by¹⁸

$$M_I = \frac{\bar{\varphi}_I}{N_I} \frac{D \cdot N_e}{k_B T} \quad (\text{III.6})$$

where D_e is the diffusion coefficient of monomers, and N_e is the effective number of monomers per entanglement length.

We solve eqs III.4 in terms of dimensionless parameters, $x = (k_B T / 2\kappa N)^{1/2} r$ and $\tau = M(k_B T)^2 t / 2\kappa N^2$, and reduced $m_{IJ} = M_{IJ}/M$ and $\bar{\kappa}_{IJ} = \kappa_{IJ}/\kappa$, where $M = (1/4N) \cdot (D \cdot N_e / k_B T)$ and $\kappa = k_B T (4a^2/36)$. The eqs III.4 in dimensionless forms are solved using the finite-difference method for the spatial and the temporal derivatives.⁹ The values of Δx and $\Delta \tau$ are chosen to simulate continuous dynamics avoiding artificial numerical slowing down effects. (Since according to eqs III.4 the local compositions $\varphi_I(r, t)$, $I = A, B$, and C , will evolve in time provided that there is a gradient in composition, the interfacial thickness should be larger than Δx .) The simulations are done in 2D. We have considered a square lattice with L^2 grids, $L = 64$. The periodic boundary conditions have been used to avoid surface effects. Since the initial high temperature state is a homogeneous mixture, the initial compositions φ_A and φ_B for each grid are chosen to be uniformly random number distributed in the interval $[\bar{\varphi}_A - \eta, \bar{\varphi}_A + \eta]$ and $[\bar{\varphi}_B - \eta, \bar{\varphi}_B + \eta]$, respectively. We choose $\eta = 0.01$ here. We have run 10 times from $\tau = 0$ up to $\tau = 2 \times 10^4$ and 10 runs are averaged. Each run is started from a different random seed (i.e., a different initial composition field over the same average fluctuation). For systems 2–5 in Figure 1, parts d and f, a time step $\Delta \tau = 0.01$ and a grid size $\Delta x = 1.2$. Since for system 1 in Figure 1d the equilibrium interfaces are broader, we choose a larger grid size, $\Delta x = 1.6$, and a time step $\Delta \tau = 0.02$.

IV. Results and Discussion

IV.a. Decomposition Patterns. The density maps of components A, B, and C for systems 1–5 are shown in Figures 2–6. In Figures 3–6, the local composition φ_I from 0.0 to 1.0 is represented as from purely white to purely red, green, and blue for $I = A, B$, and C , respectively. In Figure 2 for system 1 the color from completely white to completely red represents the local composition φ_A from minimum to maximum at that snapshot, and the same for φ_B , and φ_C , rather than using actual composition colors.

The density maps of A, B, and C as a function of time during spinodal decomposition for system 1 in Figure 1d are shown in Figure 2, parts a, b, and c, respectively. As time increases, the A-rich and B-rich regions are always identical; the system separates into A–B-rich and C-rich phases with equal amount. In general the decomposition dynamics for a ternary system with $\bar{\varphi}_A = \bar{\varphi}_B < \bar{\varphi}_C$ in Figure 1d are identical to the results for a symmetric binary system, i.e., a ternary system with

$\bar{\varphi}_A = \bar{\varphi}_B < \bar{\varphi}_C$ decomposes into a two-phase mixture in the same way as a symmetric binary system because A and B act like a single component of composition $\bar{\varphi}_A + \bar{\varphi}_B$.

On the other hand for system 2 in Figure 1d where $\bar{\varphi}_A = \bar{\varphi}_B > \bar{\varphi}_C$, the two-phase decomposition kinetics are more complicated. In Figures 3a and 3b we show that the spinodal decomposition occurs mainly along the direction to the A- and B-rich phases, and in Figure 3c we show the segregation of the minority component C in the interface between the A- and B-rich phases as a function of time. Even though the equilibrium composition of C in both phases is predicted to be equal to the average composition of C, i.e., $\bar{\varphi}_C^a = \bar{\varphi}_C^b = \bar{\varphi}_C$, we show here that the minority component C is not homogeneous. We find $\bar{\varphi}_C^a = \bar{\varphi}_C^b = \bar{\varphi}_C - \epsilon$ and the composition of C at the center of the interface $\varphi_C^M > \bar{\varphi}_C$. In order to see if this is a finite size effect, we have run the simulation doubling the size of the system, i.e., with grids $L^2 = 128 \times 128$. We find that although ϵ is smaller, φ_C^M and the interfacial thickness l are almost the same as the values with $L^2 = 64 \times 64$. Therefore as $L \rightarrow \infty$, $\epsilon \rightarrow 0$ while φ_C^M and l tend to be size-independent constants. This shows the segregation of the minority component C in the interface should be observed.

For a flat interface one can show that a net decrease of the gradients at the interface provided by an excess of minority composition decreases the specific interfacial energy of the system σ . In a flat interface between α and β of compositions $\bar{\varphi}_I^\alpha$ and $\bar{\varphi}_I^\beta$, σ is given by the difference per unit area of interface between the actual free energy and that which it will have if the properties of the two phases were continuous¹⁹

$$\sigma = N_V \int_{-\infty}^{\infty} \left(\Delta f_e^m + \sum_{I=A, B, C} \bar{\kappa}_{II} \left(\frac{d\varphi_I}{dx} \right) \right) dx \quad (\text{IV.1})$$

where N_V is the number of monomers per unit volume and

$$\Delta f_e^m = \sum_{I=A, B, C} \frac{\varphi_I(x)}{N_1} (\mu_{e,I}(\{\varphi_I(x)\}) - \mu_{e,I}(\{\bar{\varphi}_I^\alpha\})) \quad (\text{IV.2})$$

The composition of C is eliminated through the incompressibility constraint. An extremum of σ is obtained solving simultaneously the resulting two Euler–Lagrange equations,²⁰ which using the boundary conditions, Δf_e^m and $d\varphi_I/dx$ tend to zero as $x \rightarrow \pm\infty$, leads to

$$\Delta f_e^m = \kappa_{AA} \left(\frac{d\varphi_A}{dx} \right)^2 + 2\kappa_{AB} \frac{d\varphi_A}{dx} \frac{d\varphi_B}{dx} + \kappa_{BB} \left(\frac{d\varphi_B}{dx} \right)^2 \quad (\text{IV.3})$$

When the composition of the minority component C is a constant everywhere $\varphi_C(x) = \bar{\varphi}_C$, the composition profile $\varphi_C(x)$ is an extremum of σ . There are, however, many extrema of σ ; only the lowest minimum σ will give the actual interface. In general, an infinitesimal excess in $\varphi_C(x)$ can only be an extremum of σ if it breaks the symmetry, $\varphi_A(x) - \bar{\varphi}_A = \bar{\varphi}_B - \varphi_B(x)$, i.e., for a nonselective minority component, a profile $\varphi_C(x) = \varphi_C(-x)$ with $\varphi_I(x) = \varphi_I(-x) - \xi_I(x)$, $I = A, B$, must obey $\xi_A(x) \neq \xi_B(x)$ to be able to minimize σ . For example, in system 2 it is found numerically that $\xi_B(x) < 0$ and $0 < |\xi_B(x)| < \xi_A(x)$ when $x < 0$. With a linear expansion in $\xi(x)$ of the

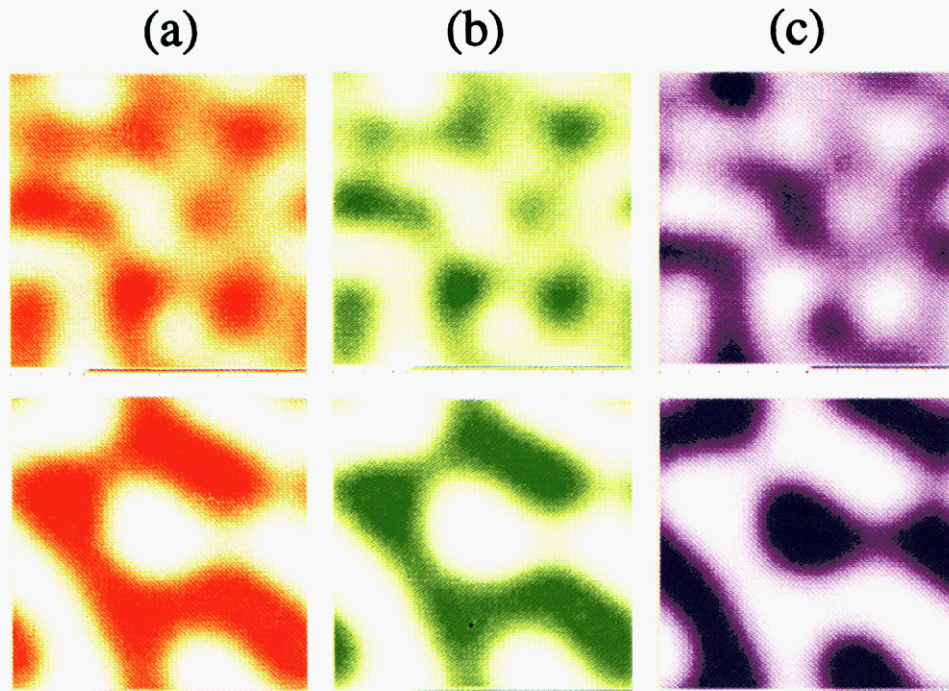


Figure 2. The density maps as a function of time for (a) component A, (b) component B, and (c) component C of system 1 in Figure 1d during the decomposition process. Rows 1 and 2 correspond to $\tau = 800$ and $\tau = 20\,000$, respectively.

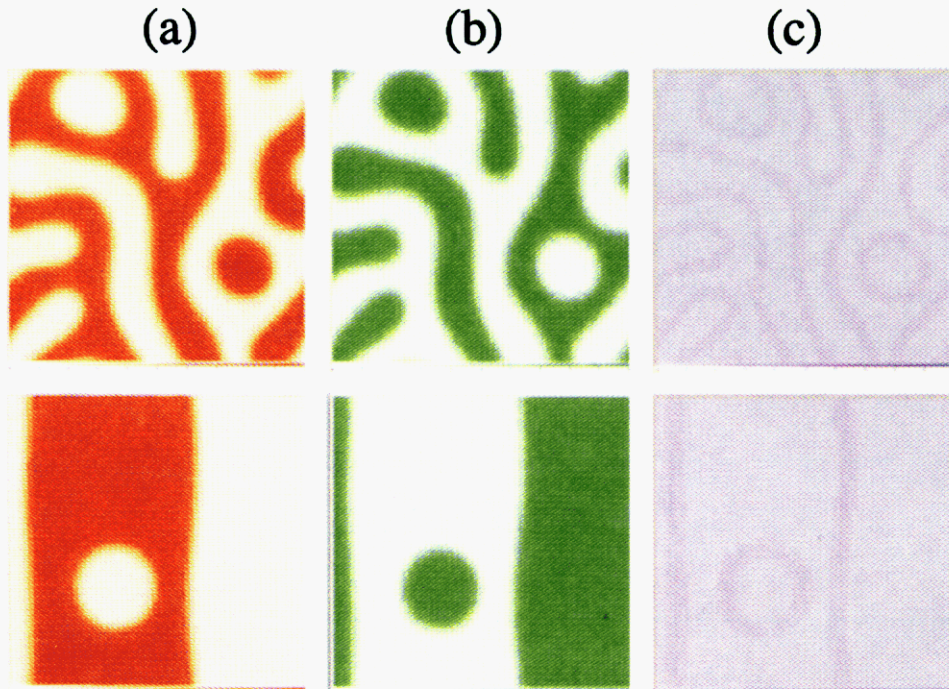


Figure 3. The density maps as a function of time for (a) component A, (b) component B, and (c) component C of system 2 in Figure 1d during the decomposition process. Rows 1 and 2 correspond to $\tau = 400$ and $\tau = 10\,000$, respectively.

integrand in eq IV.1 we find that $\xi_I(x) \neq 0$, $I = A$, or B , decreases σ . Although the resulting profile is clearly not an extremum of σ , it explains the interface segregation phenomenon observed.

The segregation of the minority component in the interface has a strong influence in the decomposition patterns of a ternary system unstable to the formation of two majority phases and metastable to the formation of a minority phase. The dynamics of system 3 in Figure 1d are shown in Figure 4, parts a, b, and c. The pattern is like that of system 2 with a thicker interface. The decomposition is driven by the instability of the system

to the formation of two majority $\alpha + \beta$ phases. Although there is segregation of the minority component C at the interface between $\alpha + \beta$, it does not lead to the formation of the δ minority phase. That is, it is not possible to distinguish a third phase from the interface in Figure 4, parts a, b, and c, because the interfacial thickness l is large and a growth of the δ phase is not observed. Since the δ phase is metastable, the formation of a nucleus of a critical size is required for the δ phase to coarsen. The closer the initial compositions to $\{\bar{q}_I^\delta\}$, the larger the critical nucleus. In the classical theory, this nucleus should be spherical (circular in 2D). Since

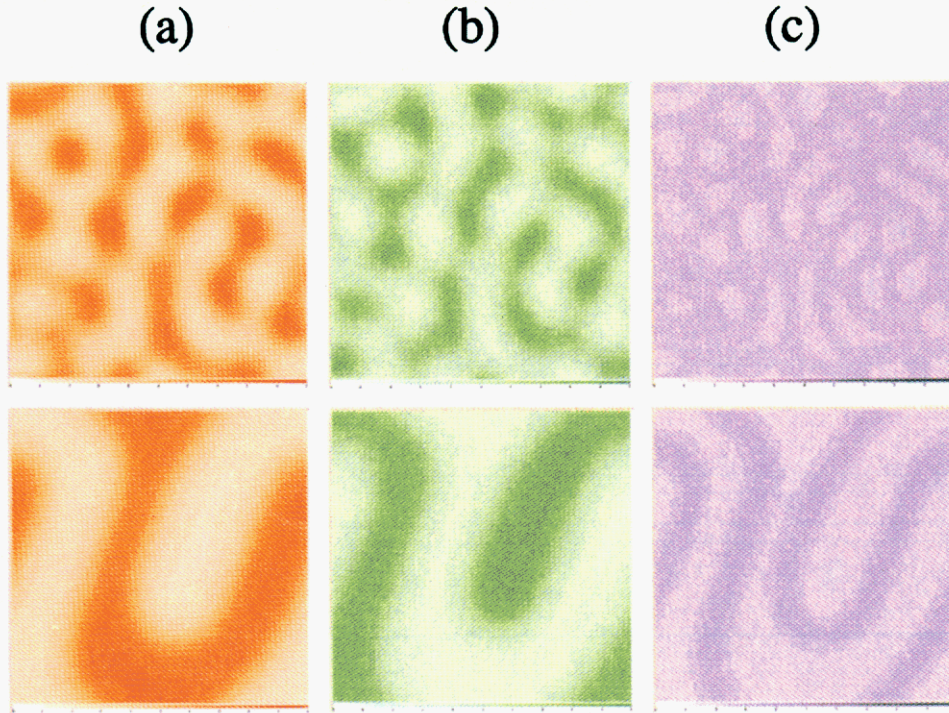


Figure 4. The density maps as a function of time for (a) component A, (b) component B, and (c) component C of system 3 in Figure 1d during the decomposition process. Rows 1 and 2 correspond to $\tau = 400$ and $\tau = 10\,000$, respectively.

the interface is rich in C, a spherical (or circular) nucleus forms only at the junction of the interfaces. For shallow quenches, however, the nucleus still cannot reach the critical size at these junctions. Therefore at this thermal energy we observe no coarsening of the third phase, and the segregation of C at the interface can be considered simply as increasing the interfacial thickness.

We study deeper quenches to determine if the minority phase can coarsen. Since the interface is sharp for deep quenches and the critical size of the nucleus to grow is small, we expect that for low enough thermal energy, the minority phase should be distinguished from the interface in the region that separates the α and β majority phases and get coarsened. In Figure 5, parts a, b, and c, we show the density maps of A, B, and C for system 4 in Figure 1f as a function of time, respectively. As shown in Figure 5, parts a, b, and c, the decomposition process occurs primarily along the direction to the A- and B-rich phases. As spinodal decomposition proceeds, α and β phases get coarsened very quickly. One can observe that the coarsening of the third minority phase is only possible when a critical volume of the minority phase forms. The critical volume is achieved at the junction of four or five domains rich in the majority components. In this case, we observe in the later stages that between any two $\beta + \gamma$ phases rich in component I and J respectively the third component K segregates in the interface. For example in Figure 5a, A segregates in the interface between the B- and C-rich phases even though the C-rich phase has the lowest volume fraction.

This segregation behavior of the third component in the interface between any two phases rich in the other two components is also observed in the dynamics for systems with two minority components, $\bar{\varphi}_A = \bar{\varphi}_B < \bar{\varphi}_C$, metastable to the formation of $\alpha + \beta$ and unstable to the formation of γ , such as system 5 in Figure 1f. The dynamics of system 5 are shown in Figure 6, parts a, b, and c. One can observe that A and B act like one com-

ponent of composition $\bar{\varphi}_A + \bar{\varphi}_B$ and the system separates into A-B- and C-rich phases for the initial decomposition stages ($\tau = 400$). At larger times ($\tau = 1600$) the $\bar{\varphi}_A + \bar{\varphi}_B$ rich regime decomposes into $\alpha + \beta$ phases.

IV.b. Scaling and Growth Behaviors. In ternary systems the structure function of the various components $S_{II}(k, \tau)$, where the other two components are assumed to have identical atomic scattering factors, are computed to determine the growth law of the segregated domains during the decomposition,

$$S_{II}(k, \tau) = \sum_{|\vec{k}|=k} S_{II}(\vec{k}, \tau) / \sum_{|\vec{k}|=k} 1 \quad (\text{IV.4a})$$

with

$$S_{II}(\vec{k}, \tau) = \left\langle \frac{1}{L^2} \sum_{\vec{r}} \sum_{\vec{r}'} e^{i\vec{k} \cdot \vec{r}} [\varphi_I(\vec{r} + \vec{r}') \varphi_I(\vec{r}') - \bar{\varphi}_I^2] \right\rangle \quad (\text{IV.4b})$$

where the sums are over all of the L^2 grids, and \vec{k} is the wave vector which belongs to the first Brillouin zone in the reciprocal space

$$\vec{k} = (2\pi/L\delta x)\vec{\theta} \quad (\text{IV.5a})$$

where

$$\vec{\theta} = (\theta_x, \theta_y) \quad \theta_x, \theta_y = 0, 1, 2, \dots, L - 1 \quad (\text{IV.5b})$$

We compute the mean magnitude of the vector $\langle k \rangle_{II}$ to determine the characteristic domain size $\langle R \rangle_{II}$

$$\langle R \rangle_{II} \sim 1/\langle k \rangle_{II} \quad (\text{IV.6a})$$

with

$$\langle k \rangle_{II} = \sum k S_{II}(k, \tau) / \sum S_{II}(k, \tau) \quad (\text{IV.6b})$$

In Figure 7, parts a and b, we plot $\langle R \rangle_{CC}$ vs $\tau^{1/3}$ and $S_{CC}(k, \tau)/\langle R \rangle_{CC}^2$ vs $k\langle R \rangle_{CC}$ for system 1 in Figure

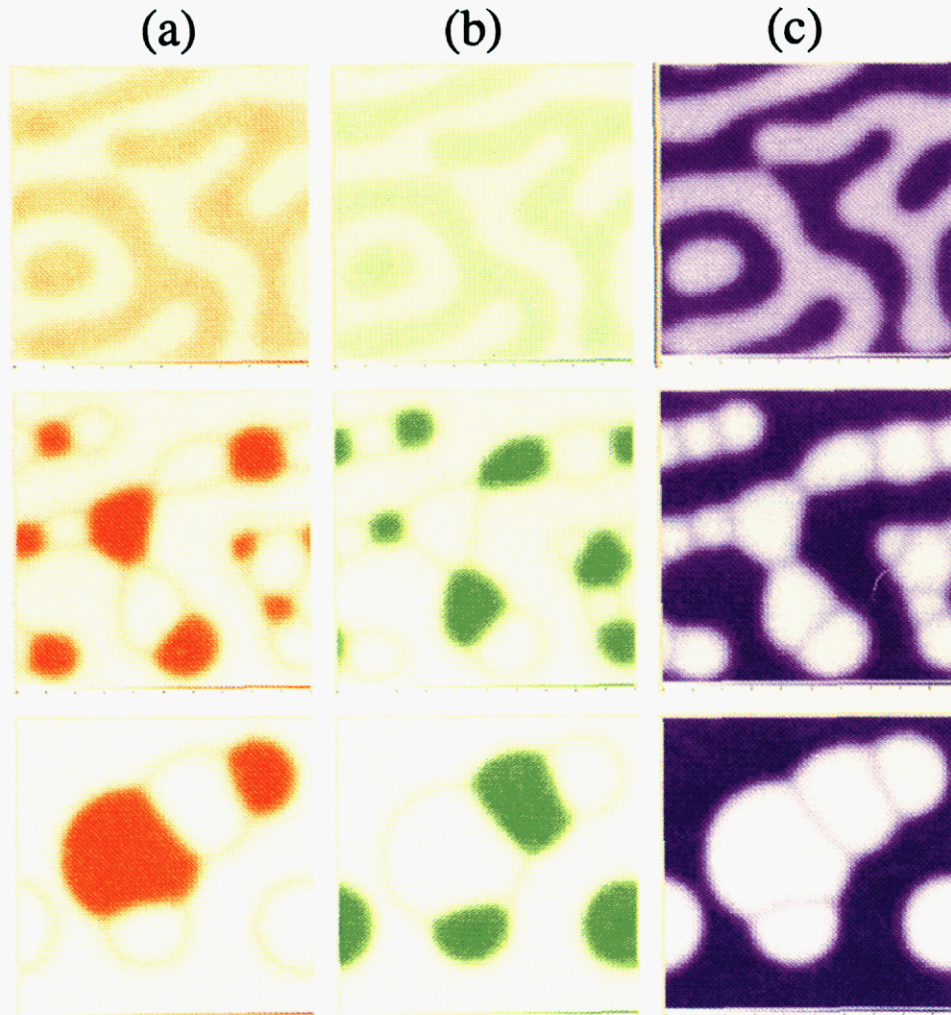


Figure 5. The density maps as a function of time for (a) component A, (b) component B, and (c) component C of system 4 in Figure 1f during the decomposition process. Rows 1, 2, and 3 correspond to $\tau = 400$, $\tau = 4000$, and $\tau = 10\,000$, respectively.

1d, respectively. We find that $S_{CC}(k, \tau)$ scales as $\langle R \rangle_{CC}^2 G(k \langle R \rangle_{CC})$ and $\langle R \rangle_{CC} \sim \tau^{1/3}$ in the scaling regime. Clearly the same results as for component C are expected for the minority components A and B. It is not surprising that the dynamical scaling law and the growth law for each component hold in this ternary system decomposing into two phases, because the dynamics are identical to the results for a symmetric binary system.

The dynamical scaling and the growth behaviors in systems decomposing into three phases, such as systems 3, 4, and 5, are analyzed below. It should be noted that the growth of the minority phase in system 3 is not analyzed since it does not coarsen as time increases. The rescaled structure functions are not self-similar while the segregation at the interface has not reached the steady state. The growth power law, however, analyzed in terms of the mean magnitude of the wave vector in eqs IV.6 is always obeyed in each system, as shown in Figure 8, parts a and b, where we plot $\langle R \rangle_{II} \sim \tau^{1/3}$ for the majority component A and the minority component C of system 4 in Figure 1f, respectively. The self-similar regime is observed at the very late stages, as shown in Figure 8, parts c and d, where we plot $S_{II}(k, \tau)/\langle R \rangle_{II}^2 \sim k \langle R \rangle_{II}$, I = A and C, respectively for system 4. This scaling regime during phase separation is obtained when the structure is self-similar. In ternary systems decomposing into three phases, the segregation at the

interface breaks the self-similarity observed even at the early stages of the decomposition in binary systems. Self-similarity is obtained when the interface segregation reaches the steady state. The steady state in ternary systems decomposing into three phases by spinodal decomposition is reached more slowly than in binary systems. These results should also be found in ternary systems with $\bar{\varphi}_A = \bar{\varphi}_B > \bar{\varphi}_C$ decomposing into two phases such as system 2 in Figure 1d, where the minority component C segregates in the interface between A-rich and B-rich phases.

V. Conclusions

The dynamics of phase separation into two and three phases of symmetric A–B–C ternary polymer blends, i.e., $\chi_{AB} = \chi_{BC} = \chi_{AC} = \chi$ and $N_A = N_B = N_C = N$, have been studied. The extra degree of freedom provided by the third component in ternary systems makes the interface between any two phases more complicated than in binary systems. We show here that between any two phases $\alpha + \beta$ rich in components I and J, respectively, the third component K segregates in the interface between $\alpha + \beta$. This interface segregation behavior is quite general; it is also observed in nonsymmetric ternary polymer blends, which will be discussed elsewhere.²¹ The segregation at the interface influences the pattern of the decomposition process. It determines the growth of a third phase with lowest volume fraction

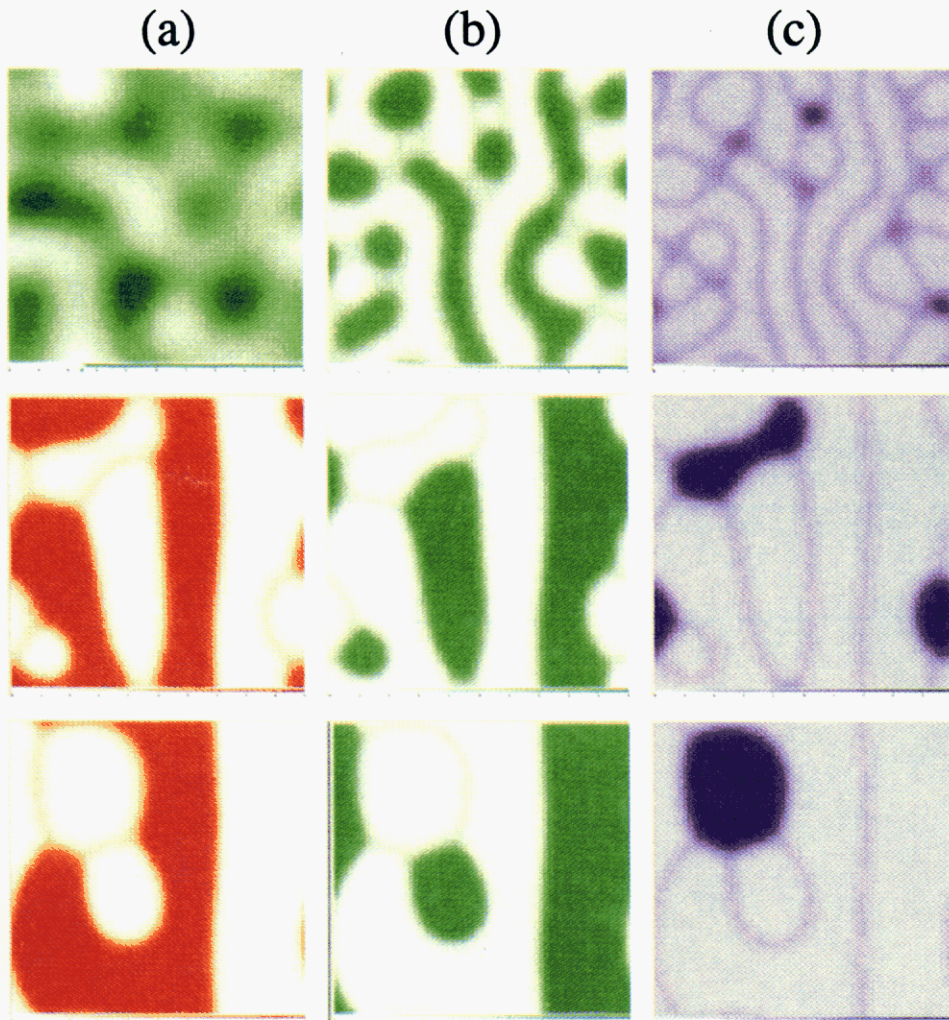


Figure 6. The density maps as a function of time for (a) component A, (b) component B, and (c) component C of system 5 in Figure 1f during the decomposition process. Rows 1, 2, and 3 correspond to $\tau = 400$, $\tau = 1600$, and $\tau = 10\,000$, respectively.

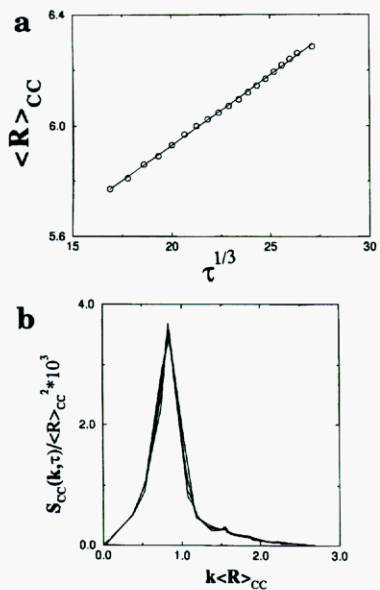


Figure 7. Plots of (a) $\langle R \rangle_{CC}$ vs $\tau^{1/3}$ and (b) $S_{CC}(k, \tau)/\langle R \rangle_{CC}^2$ vs $k\langle R \rangle_{CC}$ of system 1 in Figure 1d. $S_{CC}(k, \tau)$ and $\langle R \rangle_{CC}$ are defined in eqs IV.4 and IV.6, respectively. The scaling results shown in b are valid from $\tau = 4800$.

and turns the coarsening kinetics into a topological problem. In systems unstable to the formation of two majority phases and metastable to the formation of one

minority phase, the minority phase, formed at the interface between two majority phases, does not coarsen when the interface is very broad, it can be considered simply as increasing the interfacial thickness between the two majority phases. When the thermal energy decreases even further, since the interface is sharper in the later stages of the decomposition process, the minority phase cannot be considered any longer as thickening the interface but it appears as a new phase that separates these two majority phases. The coarsening of a third phase rich in a minority component is not always observed. It can only coarsen at the junction of multiple majority phase domain boundaries in a bicontinuous pattern²² for deeper quenches. In two dimensions the critical volume of the third phase required for its growth is achieved when four or more majority phase domain boundaries join. Therefore the incubation time for the minority phase growth is a function of the space dimensionality d . The segregation of a third component in the interface between two phases rich in the other components, however, is not expected to be a function of d in mixtures well described by mean field theories.

We find that ternary systems undergoing two-phase and three-phase separations always obey the growth law $R \sim \tau^{1/3}$ even when the decomposition patterns are not self-similar. Ternary systems, however, do reach a scaling regime at the very late stages, where the segregation of the third component in the interface

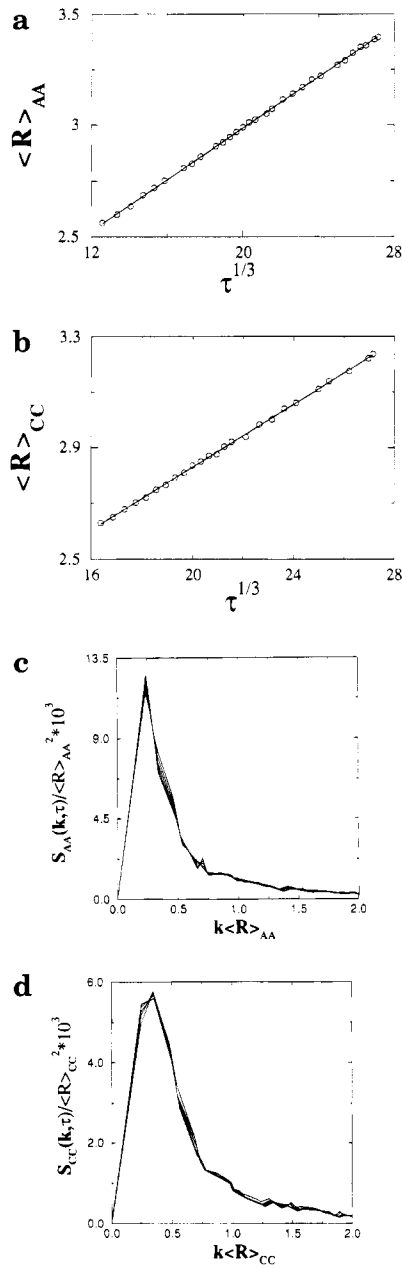


Figure 8. Plots of $\langle R \rangle_{\text{II}}$ versus $\tau^{1/3}$ for (a) I = A, (b) I = C, and $S_{\text{II}}(k, \tau) / \langle R \rangle_{\text{II}}^2$ vs $k \langle R \rangle_{\text{II}}$ for (c) I = A, (d) I = C, of system 4 shown in Figure 1f. $S_{\text{II}}(k, \tau)$ and $\langle R \rangle_{\text{II}}$ are defined in eqs IV.4 and IV.6, respectively. The scaling results shown in c and d are valid from $\tau = 8400$.

reaches the steady state. As in binary systems, the domain growth law $R \sim \tau^{1/3}$ is expected to be independent of the space dimensionality d . We neglect here the hydrodynamic flow which may lead to the domain growth $R \sim \tau$ in connected fluid microstructures.²³

Acknowledgment. We are indebted to Professor P. W. Vorhees for his many enlightening and helpful discussions. We thank Professor G. B. Olson for useful suggestions. This work was supported by the National Science Foundation (PYI Grant No. DMR 9057764), the David and Lucile Packard Foundation, and the Ford Motor Co.

Appendix A

The chemical potential of component I defined in eq II.4a, $\mu_{\circ, I}$, can be obtained using the relationships,

$$\Delta F_{\circ} = \Delta f_{\circ} \sum_I n_I N_I \quad (\text{A.1})$$

$$\varphi_I = \frac{n_I N_I}{\sum_J n_J N_J} \quad I = A, B, C \quad (\text{A.2})$$

By chain rules

$$\mu_{\circ, I} = \frac{\partial \Delta F_{\circ}}{\partial n_I} = \frac{\partial \Delta f_{\circ}}{\partial n_I} \sum_J n_J N_J + N_I \Delta f_{\circ} \quad I = A, B, C \quad (\text{A.3})$$

where

$$\frac{\partial \Delta f_{\circ}}{\partial n_I} = \sum_J \frac{\partial \Delta f_{\circ}}{\partial \varphi_J} \frac{\partial \varphi_J}{\partial n_I} \quad I = A, B, C \quad (\text{A.4})$$

with $\partial \Delta f_{\circ} / \partial \varphi_J$ and $\partial \varphi_J / \partial n_I$ obtained using eqs II.1b and A.2

$$\frac{\partial \Delta f_{\circ}}{\partial \varphi_J} = \frac{\ln \varphi_J}{N_J} + \frac{1}{N_J} + \sum_{K \neq J} \chi_{KJ} \varphi_K \quad J = A, B, C \quad (\text{A.5})$$

and

$$\frac{\partial \varphi_J}{\partial n_I} = \frac{\varphi_I (1 - \varphi_I)}{n_I} \quad J = I \quad (\text{A.6a})$$

$$\frac{\partial \varphi_J}{\partial n_I} = \frac{-\varphi_I \varphi_J}{n_I} \quad J \neq I \quad (\text{A.6b})$$

Substituting eqs A.4–A.6 into A.3, $\mu_{\circ, I}$ has the final form given by eq II.4b.

Appendix B

The total free energy of nonhomogeneous ternary polymer blends, ΔF , is given by

$$\Delta F = N_V A \int_{r_1}^{r_2} \Delta f \, dr \quad (\text{B.1})$$

where N_V is the number of sites per unit volume, A is the cross sectional area of the system, and Δf is given in eq II.1a.

For a system in equilibrium, the total free energy ΔF will be a minimum. Therefore we have to determine the variations of φ_A , φ_B , and φ_C , with respect to r which minimize ΔF with the constraints that the average compositions of A, B, and C remain constants, i.e.,

$$\int_{r_1}^{r_2} (\varphi_I - \bar{\varphi}_I) \, dr = 0 \quad I = A, B, C \quad (\text{B.2})$$

To add these constraints to the total free energy, we multiply undetermined constants λ_I , $I = A, B, C$, to eqs B.2 and subtract to the total free energy function in eq B.1. The final form is

$$I = N_V A \int_{r_1}^{r_2} (\Delta f - \sum_I \lambda_I (\varphi_I - \bar{\varphi}_I)) \, dr \quad (\text{B.3})$$

The determinations of the variations of φ_I , $I = A, B$, and C with respect to r are obtained from²⁰

$$\frac{\partial I}{\partial \varphi_I} - \nabla \left(\frac{\partial I}{\partial \nabla \varphi_I} \right) = 0 \quad I = A, B, C \quad (B.4)$$

Therefore

$$\lambda_I = \frac{\partial \Delta f^*}{\partial \varphi_I} - 2\bar{\kappa}_{II} \nabla^2 \varphi_I \quad I = A, B, C \quad (B.5)$$

where $\partial \Delta f^*/\partial \varphi_I$ is given in eq A.5, and $\bar{\kappa}_{II}$ is in eq II.2.

It is apparent that λ_I in eq B.5 is the chemical potential of component I per site, μ_I^s , in nonhomogeneous systems.

References and Notes

- (1) Binder, K.; Stauffer, D. *Phys. Rev. Lett.* **1974**, 33, 1006. For a review, see: Gunton, J. D.; San Miguel, M.; Sahni, P. S. In *Phase Transitions and Critical Phenomena*; Domb, C., Lebowitz, J. L., Eds.; Academic: London, 1983; Vol. 8.
- (2) Chen, L. Q. *Scri. Metall. Mater.* **1993**, 29, 683. Chen, L. Q. *Acta Metall. Mater.* **1994**, 42, 3503.
- (3) Jeppesen, C.; Mouritsen, O. G. *Phys. Rev.* **1993**, B47, 14724. Laradji, M.; Mouritsen, O. G.; Toxvaerd, S. *Europhys. Lett.* **1994**, 28, 157.
- (4) Edwards, S. F. *J. Phys.* **1975**, A8, 1670.
- (5) de Gennes, P. G. *J. Phys. (Paris) Lett.* **1977**, 38, 441. de Gennes, P. G. *Scaling Concepts in Polymer Physics*; Cornell Univ. Press: Ithaca, NY, 1979.
- (6) de Gennes, P. G. *J. Chem. Phys.* **1980**, 72, 4756.
- (7) Scott, R. L. *J. Chem. Phys.* **1949**, 17, 279.
- (8) Tompa, H. *Trans. Faraday Soc.* **1949**, 45, 1142.
- (9) Chakrabarti, A.; Toral, A.; Gunton, J. D.; Muthukumar, M. *Phys. Rev. Lett.* **1989**, 63, 2072.
- (10) de Gennes, P. G. *J. Phys. (Paris) Lett.* **1979**, 40, 69.
- (11) We neglect the contribution to $\bar{\kappa}_{II}$ from the short range van der Waals interactions because in polymers it is $1/N$ smaller than the contribution from the chain connectivity; see ref 19.
- (12) For a comparison, we numerically solve the nonlinear diffusion equations of system 2 shown in Figure 1d using the exact forms of $\bar{\kappa}_{II}$.
- (13) de Fontaine, D. Doctoral dissertation, Northwestern University, Evanston, IL, 1967.
- (14) Rogers, T. M.; Elder, K. R.; Desai, C. *Phys. Rev.* **1988**, B37, 9638.
- (15) Kramer, E. J.; Green, P.; Palstrom, C. *J. Polymer* **1984**, 25, 473.
- (16) Composto, R. J.; Kramer, E. J.; White, D. M. *Nature* **1987**, 328, 234.
- (17) In polymer blends of comparable molecular weights, the results of Kramer and de Gennes are similar (see discussions in the paper of J. Rhee and B. Crist (*Macromolecules* **1991**, 24, 5663)).
- (18) de Gennes, P. G. *J. Chem. Phys.* **1971**, 55, 572.
- (19) Cahn, J. W.; Hilliard, J. E. *J. Chem. Phys.* **1958**, 28, 258.
- (20) Hildebrand, F. B. *Methods of Applied Mathematics*; Prentice-Hall: New York, 1992.
- (21) Huang, C.; Olvera de la Cruz, M.; Voorhees, P. W. Manuscript in preparation.
- (22) In the presence of hydrodynamic flow which we neglect here the growth of the third minority phase can be much faster through flow of materials from thin to thick regions via Tomita instabilities; see ref 23.
- (23) McMaster, L. P. *Adv. Chem. Ser.* **1975**, 142, 43. Siggia, E. *D. Phys. Rev.* **1979**, 20A, 595.

MA950497A